Journal of Catalysis **209,** 501–514 (2002)
doi:10.1006/jcat.2002.3647

The Interaction of Hydrogen with Ru/MgO Catalysts

C. Zupanc, A. Hornung, O. Hinrichsen,[1] and M. Muhler

Laboratory of Industrial Chemistry, Ruhr-University Bochum, D-44780 Bochum, Germany

Received January 31, 2002; revised April 18, 2002; accepted April 18, 2002

The energetics of the interaction of hydrogen with MgO-supported Ru catalysts (Ru/MgO, Cs–Ru/MgO) was studied by combining temperature-programmed (TP) techniques, volumetric hydrogen chemisorption, and microkinetic modeling. Various TP experiments (TP desorption, TP adsorption) were carried out, applying different H_2 dosing procedures (isothermal flow experiments, pulse flow chemisorption, etc.). The interaction of H_2 with a Ru/MgO catalyst can be rationalized as follows: hydrogen preferentially dissociates on low-coordinated defectlike sites ("portal"-mediated adsorption). These species migrate to high-energy sites and subsequently fill up via diffusion the intermediate-energy and then the low-energy sites. Furthermore, a direct adsorption pathway on the different Ru sites was identified. Results obtained by volumetric hydrogen chemisorption performed at different temperatures correlate well with the amount detected in the TP experiments. By means of microkinetic modeling, the peaks in the obtained TPD signal could be assigned to the desorption from different Ru single-crystal surfaces. On Cs–Ru/MgO, the dopant was found to block the portal sites suppressing the fast nonactivated adsorption path.

1. INTRODUCTION

The interaction of hydrogen with ruthenium plays an important role in numerous industrial heterogeneously catalyzed hydrogenation reactions. In Fischer–Tropsch synthesis, Ru is one of the most active metal components (1–3). In contrast to Fe or Co, Ru favors the formation of high-molecular-weight hydrocarbons from synthesis gas at lower reaction temperatures (1). The Kellogg Brown & Root Advanced Ammonia Process (KAAP) (4–8) employs a catalyst made of Ru on a graphite support (Ru/C). Recently, barium-promoted Ru catalysts were developed with unprecedented activity and stability (9, 10). Methanization from CO and H_2 (11, 12), the selective catalytic reduction of NO (SCR) (see (13) and references therein), and the conversion of benzene and its derivatives to cyclohexene and relevant cycloalkenes (14–16) are counted, among other applications of supported Ru, as a heterogeneous hydrogenation catalyst.

[1] To whom correspondence should be addressed. E-mail: olaf@techem.ruhr-uni-bochum.de.

The kinetics of adsorption and desorption of H_2 has been investigated on Ru single crystals by various research groups very extensively (17–32). In particular, the basal Ru(0001) surface was subjected to many studies employing a large variety of experimental surface science tools, such as low-energy electron diffraction (LEED), video LEED (VLEED), high-resolution electron energy loss spectroscopy (HREELS), angle-resolved ultraviolet photoelectron spectroscopy (ARUPS), thermal desorption spectroscopy (TDS), and work function measurements. In TDS, at low initial coverages of hydrogen, desorption leads to a single high-temperature peak, which was found to shift from 470 to 380 K with increasing initial hydrogen coverage (23, 31). At higher exposures a second desorption peak was observed with a peak temperature of 320 K, indicating a strong deviation from the characteristic Langmuirian second-order desorption. The maximum coverage of hydrogen (Θ_H) using gas-phase atomic hydrogen (33) was found to be 1.42 hydrogen atoms per primitive Ru(0001) unit cell, in contrast to the one adatom per unit cell obtained by dissociative chemisorption of molecular hydrogen (30). At low coverages, hydrogen occupies the fcc threefold hollow sites on Ru(0001), as identified by HREELS (30). At saturation coverage, hydrogen was found to sit additionally on sites of slightly reduced symmetry. This phenomenon resulted either from reconstruction of the Ru surface or from movement of the hydrogen adatoms toward the bridge position (30). The low-temperature desorption peak can be correlated with these less strongly bound hydrogen species. Jachimowski *et al.* (31) explained the formation of this peak in terms of coverage-dependent, repulsive interactions between nearest-neighbor and next-nearest-neighbor hydrogen atoms in the adsorbate layer. By means of a lattice gas model ($\Theta_H \leq 1$) and a mean-field approximation ($1 < \Theta_H < 1.42$) the TD spectrum for Ru(0001) was calculated; it agrees well with the experimental profile and the peak positions (31). The isosteric peak analysis yielded an activation energy of hydrogen desorption, E_{des}, on Ru(0001) that increases from ~80 ($1 \leq \Theta_H \leq 1.42$) to ~125 kJ mol^{-1} ($\Theta_H = 1$) (31). Similar results have been obtained by different research groups (22, 30).

The interaction of H_2 with the Ru(10$\bar{1}$0) surface was studied by Christmann and Muschiol (34) by means of video

0021-9517/02 $35.00

LEED, HREELS, TDS experiments, and work function measurements. They found an extremely high saturation coverage of $\Theta_H = 2$, with an initial sticking probability of $s_0 = 1$. The TD saturation spectra revealed a fairly sharp low-temperature state (peak at around 220 K) and a high-temperature state (peak at around 350 K), while at intermediate temperatures one can distinguish two other states. The adsorption energies for the four hydrogen binding states range between 56 and 80 kJ mol^{-1}. On this rough and open surface hydrogen can occupy threefold and twofold coordinated sites (27, 34–36).

In a recent experimental TDS and HREELS study, Fan and Jacobi [32] showed that hydrogen is adsorbed on the very open Ru(11$\bar{2}$1) surface in three different states, termed α-H, β-H, and γ-H. The TD spectrum displayed a desorption maximum at 345 K (γ-H); with increasing hydrogen exposure a second broad desorption peak appeared in the range 280–175 K (β-H), and at even higher hydrogen exposures a third peak was detected at 100 K (α-H) (37). Based on the interpretation of the spectra they concluded that the threefold sites are filled prior to the fourfold sites.

Detailed work on the interaction of H_2 with supported Ru catalysts was done by the King group, who applied microcalorimetry and IR and NMR spectroscopies (38–44), as well as by the Aika group (45, 46), who performed a combined IR and steady-state kinetic study. Much attention was paid to the model system Ru/SiO_2 (38–44). By means of *in situ* ^{1}H exchange NMR spectroscopy a strongly bound, immobile hydrogen species, termed α_1, and two mobile species, termed α_M and β, were detected. The β hydrogen was described as an intermediate or precursor adsorption state between the gas-phase hydrogen and the chemisorbed α species, probably sitting on low-coordinated edge and corner Ru atoms (38, 41). It was possible to correlate these three hydrogen species with results obtained by microcalorimetric measurements. Narayan *et al.* (40) determined an initial heat of adsorption of about 90 kJ mol^{-1}. With increasing hydrogen coverage a Z-shaped curve of the heat of adsorption vs Θ_H with two further plateaus was detected which can be correlated to an intermediate adsorption state (50 kJ mol^{-1}) and a weakly bound state on Ru/SiO_2 (7 kJ mol^{-1}). By means of FTIR spectroscopy applied to a Ru/MgO catalyst, hydrogen was found to adsorb dissociatively on on-top sites, bridging sites, and threefold sites (45, 46).

In our laboratory, a systematic study was performed aimed at obtaining a detailed understanding of the hydrogen adsorption and desorption kinetics for MgO-supported Ru catalysts by applying various temperature-programmed (TP) techniques. The applicability of these TP techniques compared to volumetric hydrogen chemisorption as a standard procedure to determine metal surface areas was studied from a methodical point of view (Fig. 1). Moreover, the influence of a thermal treatment on the properties of the Ru/MgO catalyst (e.g., metal particle size) and its effect on the adsorption of hydrogen were investigated. In order to bridge the material and pressure gaps between heterogeneous catalysis and surface science studies, a thorough microkinetic analysis of the experimental data was performed. Thus, we were able to correlate the detected hydrogen species (represented by the desorption peaks in the TPD spectra) to the desorption from different Ru single-crystal surfaces.

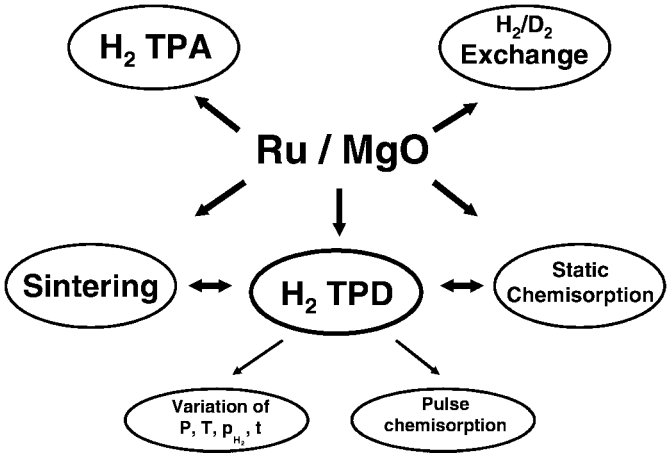

FIG. 1. Schematic of the interplay of various experiments.

2. EXPERIMENTAL

2.1. The Setup for Kinetic Measurements

The TP experiments were carried out in an all-stainless-steel microreactor setup equipped with a quadrupole mass spectrometer (GAM 445, Balzers) for fast quantitative and online measurement in the parts-per-million region. Since the setup was described in detail in a previous publication (47), only a brief summary is given here. The setup was equipped with four gas lines for helium, nitrogen, hydrogen (all 99.9999%, Messer Griesheim), and ammonia synthesis feed gas (25% N_2 in H_2; 99.999%, Messer Griesheim). The feed gas was additionally purified by means of a self-designed guard reactor to avoid any contamination of the catalyst surface. Four- and six-port switching valves (Valco) allowed a fast, back-mixing free switch between the different gas flows. H_2 pulses were introduced into the He flow by a dosing loop ($V = 50$ µl). A glass-lined stainless-steel U-tube of 3.8-mm inner diameter was used as a microcatalytic fixed-bed reactor housed in a copper jacket to achieve an isothermal catalyst bed. Additional analysis of the effluent ammonia concentration was performed by a calibrated, nondispersive infrared detector (BINOS 4b.1, Fisher–Rosemount).

2.2. Preparation and Characterization of the Catalysts

Ru/MgO catalysts were prepared by wet impregnation (imp) of high-purity MgO (Johnson–Mattey, 99.9955%) with a solution of $Ru_3(CO)_{12}$ (Strem, 99%) in absolute tetrahydrofurane (Merck, p.a.) based on the procedure described in Ref. (48). At this point a comment on the significance of the Ru precursors should be permitted: from the literature it is known that chlorine acts as a severe poison in ammonia synthesis over supported Ru catalysts (49–51). The addition of chlorine to chlorine-free precursors was found to create about six activated adsorption sites for hydrogen per chlorine adatom. Thus, in the present work, as in other recent kinetic studies by our group (9, 52, 53), the preparation of Ru/MgO was carried out with chlorine-free Ru-complex compounds. Further details of the catalyst preparation are given in Ref. (54). Recently, Bielawa *et al.* [9] obtained stable catalysts with comparable catalytic activity by intensive mixing of the precursor compounds instead of wet impregnation, followed by chemical vapor deposition (CVD) in high vacuum.

The alkali-promoted catalyst Cs–Ru/MgO (nominal 5 wt% Ru, Cs : Ru = 1 : 1) was prepared by nonaqueous impregnation using a solution of Cs_2CO_3 (ultrapure, Johnson Matthey) in absolute ethanol. After stirring the suspension for 3 h, the solvent was evaporated and the catalysts were dried in a vacuum.

In the following we present characterization results for one reference catalyst (3.3 wt% Ru/MgO) which was utilized throughout the kinetic study. Elemental analysis was performed by inductively coupled plasma optical emission spectroscopy (ICP–OES), yielding a total amount of ruthenium of 3.3 ± 0.1 wt%. The total surface area was determined in an Autosorb 1-C setup (Quantachrome) to be 50 $m^2\ g_{cat}^{-1}$ by using the standard BET method (for comparison, pure MgO is 51 $m^2\ g^{-1}$). The specific active metal surface area is determined commonly by using selective chemisorption of probe molecules such as hydrogen, oxygen, carbon dioxide, or nitrogen oxide. In our study, volumetric hydrogen chemisorption was applied using varying dosing temperatures. Based on a Ru : H stoichiometry of 1 : 1 (55–57), the specific metal surface area was determined to be 12 $m^2\ g_{cat}^{-1}$. Assuming spherical particles, an average particle size of 1.3 nm was calculated, yielding a dispersion of 75%. *Ex situ* X-ray diffraction (XRD) patterns were acquired by use of a Siemens D500 diffractometer and Cu $K\alpha$ radiation. The size of the Ru metal particles was estimated by means of a *line broadening analysis* of the ruthenium reflexes based on the Scherrer equation.

2.3. Activity Measurements

Additional catalytic tests were performed to ensure the absence of limitations by heat or mass transport under the applied experimental reaction conditions. In general, 200 mg of the 250- to 355-μm sieve fraction was placed between two quartz plugs in the outlet shank of the U-tube. Prior to each experiment, the catalyst was reduced and activated by heating it *in situ* in ammonia synthesis feed gas and ramping the temperature at 2 K min^{-1} to 783 K, followed by cycling the temperature stepwise between 588, 663, and 783 K for 2 h each overnight. This procedure ensured that the catalyst maintained the same catalytic activity and was in a well-defined state prior to the experimental TP studies.

2.4. The Temperature-Programmed Experiments

Prior to each experiment, activity measurements were performed as described in the previous section. An adsorbate-free catalyst surface was achieved by flushing the catalyst in He at 783 K for at least 1 h (Q = 100 ml (STP) min^{-1}). The catalyst was then cooled to the desired dosing temperature (T_{ads}) in He flow (Q = 50 ml (STP) min^{-1}).

Saturation with adsorbed atomic hydrogen was achieved by a flow of pure H_2 in the whole temperature range starting at 300 K, followed by cooling to 78 K. Then, the catalyst was flushed in He for half an hour. For practical reasons, 78 K was chosen, since the reactor can be easily cooled in a liquid nitrogen bath. Finally, the temperature was increased linearly using He as carrier gas. In the following, this pretreatment is referred to as the *standard* TPD experiment. In order to vary the initial coverage of adsorbed atomic hydrogen on the catalyst surface prior to the TPD experiments, different dosing procedures were applied. In the flow mode, the dosing time at a given temperature, the dosing temperature, and the partial pressure of H_2 in the gas phase diluted with He as balance gas were varied in order to collect a wide TPD database for microkinetic modeling. Furthermore, the H_2 pulse flow chemisorption allowed us to control the amount of dosed hydrogen reliably and reproducibly. After dosing H_2 with one of the above described methods, the reactor was flushed in a He flow at the dosing temperature in order to remove residual gas-phase hydrogen. Then, the catalyst was heated to 783 K at a linear heating rate of 2, 5, or 10 K min^{-1} (TPD experiments; cf. Fig. 2). In general, the temperature-programmed adsorption (TPA) experiments were carried out by flowing a mixture of diluted H_2 in He (here, 2300 ppm H_2 in He) over the reduced adsorbate-free catalyst. The temperature was kept constant at 78 K for a few minutes and then it was linearly increased to 783 K at a heating rate of 2, 5, or 10 K min^{-1}.

2.5. The Volumetric H_2 Chemisorption Experiments

Volumetric hydrogen chemisorption was applied as a standard technique to extrapolate to the monolayer of adsorbed hydrogen and to determine the specific metal surface area (58). Prior to the volumetric H_2 chemisorption measurements, the catalyst was placed in a quartz cell

between two quartz wool plugs. Reduction and activation was carried out in ammonia synthesis feed gas (gas flow, 45 ml (STP) min^{-1}) by heating the catalyst at 2 K min^{-1} to 783 K. The gases used for dosing and flushing had all a purity of 99.9999%; the feed gas (99.9995%) was additionally purified by an oxysorb cartridge. Subsequently, the setup was evacuated for at least 2 h in order to achieve an adsorbate-free reduced catalyst surface. Since we refer to results obtained by volumetric H_2 chemisorption, a detailed introduction into the procedure applied in our study and into the terminology used is given here. The measurements were carried out according to the procedure described in Refs. (55, 58): at first H_2 was dosed stepwise by 10 KPa to a final pressure of 100 kPa. The uptake of H_2 is equal to the total amount of so-called *combined* chemisorption isotherm. The cell was then evacuated and H_2 was again introduced stepwise into the cell. The measured amount of the further H_2 uptake is termed *weak*. The difference between the combined and the weak value yields the amount of so-called strongly bound hydrogen, i.e., those hydrogen species that remain on the catalyst surface while the cell is evacuated. The linear portion of the combined adsorption isotherm above $p_{H_2}/p_0 = 0.3$ was extrapolated to zero pressure (back-extrapolation method (58)), and the zero-pressure intercept was taken as the monolayer of adsorbed hydrogen (55). The results of the volumetric chemisorption on various catalysts at 300 K and on the reference catalyst at different T_{ads} are summarized in Tables 1 and 2, respectively.

2.6. Thermal Treatment of the Catalyst

In order to investigate the influence of thermal treatment on the properties of the Ru/MgO catalyst, 200 mg of a fresh sample was heated in a silica-glass tube in ammonia synthesis feed gas to temperatures between 573 and 1330 K (heating rate, 2 K min^{-1}). Subsequently, a *standard* H_2 TPD experiment was carried out. Finally, the catalyst was characterized by means of XRD, BET measurements, volumetric hydrogen chemisorption measurements, and transmission electron microscopy (Hitachi TEM H 8100).

TABLE 1

Results Obtained by Volumetric Chemisorption at $T_{ads} = 300$ K

Catalyst	Combined (μmol H_2 g_{cat}^{-1})	Weak (μmol H_2 g_{cat}^{-1})	Strong (μmol H_2 g_{cat}^{-1})	n_{des} (μmol H_2 g_{cat}^{-1})
3.3 wt% Ru/MgO (imp)	124	31	93	89
4.3 wt% Ru/MgO (imp)	157	35	122	116
1.7 wt% Ru/MgO (CVD)	66	15	51	58
0.9 wt% Ru/MgO (CVD)	33	8	25	18

Note. n_{des} specifies the amount of H_2 desorbed in TPD experiment above 300 K.

TABLE 2

Results Obtained by Volumetric Chemisorption on 3.3 wt% Ru/MgO (imp) at Different Dosing Temperatures

T_{ads} (K)	Strong (μmol H_2 g_{cat}^{-1})	Weak (μmol H_2 g_{cat}^{-1})	Combined (μmol H_2 g_{cat}^{-1})
80	124	97	221
193	98	23	121
300	93	31	124
459	49	52	101
480	46	56	102
493	42	52	94

3. RESULTS

3.1. Temperature-Programmed Methods

The temperature-programmed desorption of hydrogen (H_2 TPD) was applied as the central probe experiment (cf. Fig. 1). Pretreatment process parameters such as the total dosing pressure, the dosing temperature, the partial pressure of hydrogen, and the dosing time were varied. Pulse chemisorption was used in order to obtain TPD spectra varying from low to saturation coverage of adsorbed hydrogen. The kinetics of the interaction of hydrogen with Ru/MgO catalysts was analyzed in detail by means of TPD, TPA, and the isotopic exchange of a H_2/D_2 mixture. Moreover, the effect of sintering on the adsorption of H_2 was investigated.

3.1.1. Standard H_2 TPD experiment. Figure 2 displays the desorption spectra obtained by performing the *standard* H_2 TPD experiment with three different heating rates (2, 5, and 10 K min^{-1}). Three well-resolved signal maxima can be observed: a sharp, abruptly rising peak with an onset

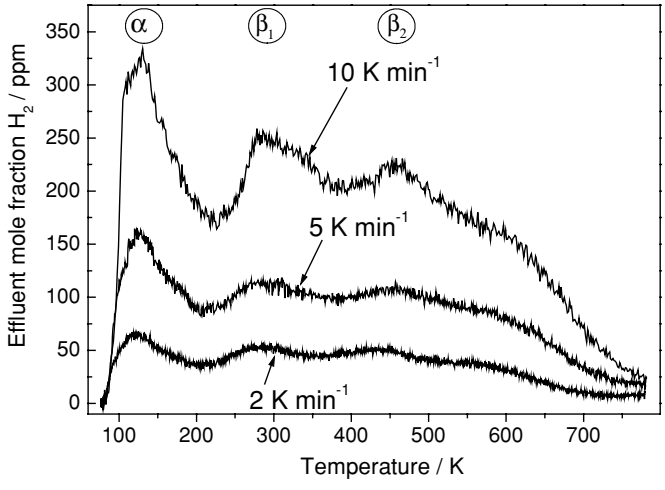

FIG. 2. Standard TPD experiments obtained with the 3.3 wt% Ru/MgO catalyst applying a heating rate of 2, 5, and 10 K min^{-1}. Experimental conditions: $Q_{He} = 50$ ml (STP) min^{-1}.

temperature below 78 K and a maximum at 120 K (very weakly bound hydrogen), a second one with a maximum temperature at 300 K (weakly bound hydrogen), and a broad peak at around 450–600 K (strongly bound hydrogen). For the sake of clarity, the three desorption states are referred to as α, β_1, and β_2 hydrogen, respectively. The upper temperature limit for the experiments was kept below 783 K in order to avoid sintering of the Ru metal particles. Above this temperature the mobility of the metal atoms increases significantly and the particle size may grow by sintering processes. From Fig. 2 it can be seen that the traces have not reached their base lines at 783 K. Obviously, at this temperature the desorption is not yet complete. Hence, integration for the determination of the total amount of adsorbed H_2 was performed in the time regime by waiting at 783 K until the desorption process was finished. The total amount of desorbed H_2 was determined to be 144 μmol g_{cat}^{-1}. The total amount can be roughly divided into three fractions: α, 25%; β_1, 27%; and β_2, 48%. When dosing H_2 on Ru/MgO catalysts containing 0.9, 1.7, 3.3, and 4.3 wt% Ru, the detected TPD spectra, shown in Fig. 3, displayed a similar signal form with related peak positions. The amount of desorbed H_2 correlated well to the Ru loading of each catalyst, which, in turn, agreed well with the amount for a monolayer of hydrogen determined by volumetric H_2 chemisorption (33, 66, 124, and 157 μmol g_{cat}^{-1}, respectively).

3.1.2. Temperature-programmed adsorption (TPA) experiments. In order to study the interaction of H_2 with the catalysts in more detail, TPA experiments were carried out using a diluted mixture of 2300 ppm H_2 in He. For closer inspection of the adsorption process, the TPA spectrum is displayed in Fig. 4 as a function of time: when switching the

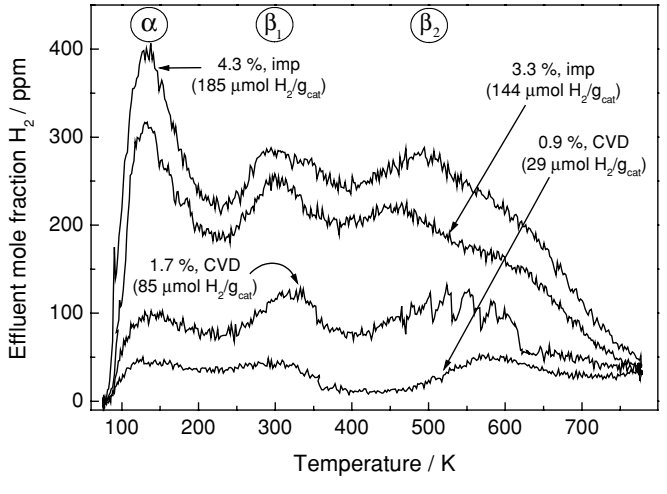

FIG. 3. Standard H_2 TPD spectra for Ru/MgO catalysts with different Ru loading (imp, prepared by impregnation; CVD, prepared by intensive mixing of the precursor compounds followed by chemical vapor deposition (CVD) in high vacuum). Experimental conditions: $\beta = 10\,\mathrm{K\,min^{-1}}$; $Q_{He} = 50$ ml (STP) $\mathrm{min^{-1}}$.

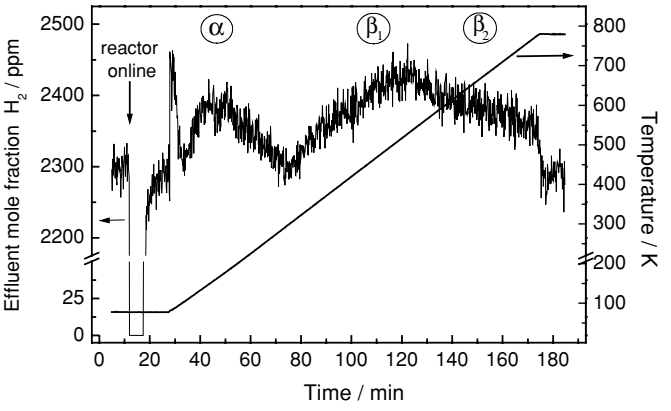

FIG. 4. Temperature-programmed H_2 adsorption experiment. Experimental conditions: 2300 ppm H_2/He; $\beta = 5\,\mathrm{K\,min^{-1}}$; $Q_{total} = 38$ ml (STP) $\mathrm{min^{-1}}$.

reactor online in the gas mixture at 78 K (Q = 38 ml (STP) $\mathrm{min^{-1}}$) hydrogen was immediately adsorbed dissociatively on the surface. It was demonstrated by an isotopic exchange flow experiment that H_2 adsorption is indeed a dissociative process in our investigated catalyst system: while flowing a diluted H_2/D_2 mixture in He over the Ru/MgO catalyst under steady-state reaction conditions at 78 K, the formation of HD reached equilibrium conversion immediately. The measured uptake of 119 μmol H_2 g_{cat}^{-1} is smaller than that in the *standard* TPD experiment by 25 μmol H_2 g_{cat}^{-1}. An additional uptake of H_2 at temperatures above 78 K was not observed. This proves clearly that the adsorption of H_2 is a nonactivated process on Ru/MgO.

In a TPA experiment, the hydrogen partial pressure (224 Pa) in the gas phase is kept higher in contrast to the experimental conditions run in the TPD experiments (maximum, 4 Pa). Therefore, the shape of the TPA spectra in Fig. 4 is even more dominated by readsorption. A shift of the TPA data points by the experimental baseline (2300 ppm) allows a direct comparison with the traces in the TPD experiment (cf. Fig. 5). In contrast to the TPD spectra, the peaks assigned to α, β_1, and β_2 hydrogen were strongly broadened and shifted by 20 (α), 80 (β_1) and 100 K (β_2) to higher temperatures. The observed shifts in the TPA experiment also demonstrate the above-mentioned increasing importance of readsorption with decreasing hydrogen coverage at higher temperatures. Due to the higher hydrogen partial pressure, additional α hydrogen was detected in the TPA spectra as a very sharp peak at the beginning of the heating rate (Fig. 4). Contrary to the standard H_2 TPD experiment, this contribution from the very weakly bound α species was probably not detected, because, due to the lower partial pressure, desorption already took place, at 78 K, while flushing the setup with He.

3.1.3. H_2 TPD experiments subsequent to dosing H_2 at 78 K. Hydrogen was adsorbed at 78 K by means of three

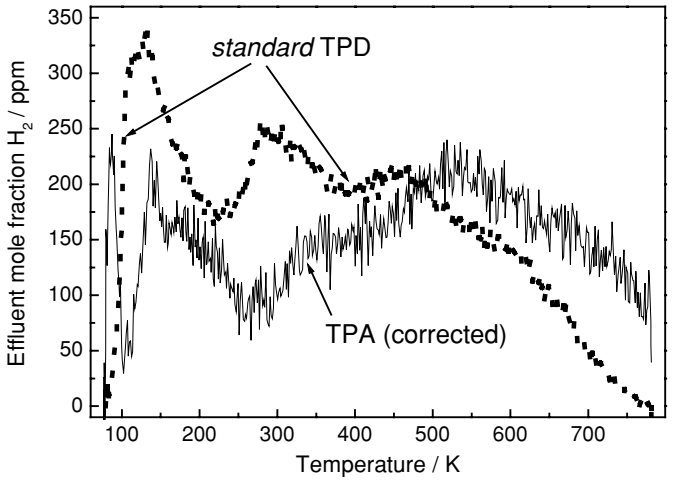

FIG. 5. Comparison of the standard H_2 TPD and TPA results.

techniques: (a) an isothermal H_2 flow experiment until saturation was obtained, (b) a pulse-flow H_2 chemisorption, and (c) isothermal H_2 flow experiments varying either the hydrogen partial pressure in the flow or the dosing time as described in the experimental section.

Figure 6 displays the TPD spectra measured after dosing pure H_2 at 78 K (black trace A) compared to the standard H_2 TPD experiment. The peaks of α and β_1 hydrogen became smaller while the desorption peak of the β_2 hydrogen remained constant. Integration yielded a total amount of 118 μmol g_{cat}^{-1}, which was 26 μmol g_{cat}^{-1} (20%) less than in the standard H_2 TPD spectrum. The additional uptake of H_2 in the latter experiment can be explained by a slow adsorption process with a low activation energy barrier for the adsorption, E_{ads}, which is surmounted when H_2 is dosed in the whole temperature range by cooling from 300 to 78 K prior to the TPD experiment. Thus, additional α and β_1 hydrogen can subsequently desorb from open surfaces. Neither an increase in the dosing pressure of H_2 up to 2.2×10^6 Pa (black trace B) nor a prolongation of the adsorption time up to 20 min at atmospheric pressure (not shown here) had any influence on the subsequent TPD profiles. This also shows that, in fact, the adsorption essentially is a nonactivated process and, consequently, the catalyst surface is readily saturated by cooling in H_2 to 78 K. The amount of H_2 detected in the TPD spectrum subsequent to dosing of H_2 at 78 K corresponds well to the one shown in the TPA spectra (Fig. 4; 118 μmol H_2 g_{cat}^{-1}), since both types of operation are comparable.

Pulse-flow H_2 chemisorption was performed in order to achieve different initial values of Θ_H for a series of subsequent TPD experiments (Fig. 7a). The shape of the TPD profiles resembles one of breakthrough curves. With an increasing number of pulses the onset of the subsequent TPD traces shifts toward lower temperatures until a similar TPD

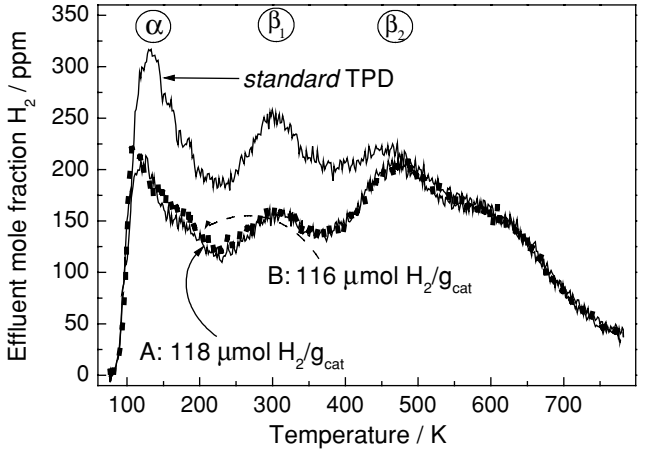

FIG. 6. TPD experiments subsequent to dosing of H_2 at 78 K using different pretreaments: A: T_{ads} = 80 K; t_{ads} = 1 min; p_{H_2} = 0.1 MPa. B: T_{ads} = 80 K; t_{ads} = 10 min; p_{H_2} = 2.2 MPa. Experimental conditions: β = 10 K min^{-1}; Q_{He} = 50 ml (STP) min^{-1}.

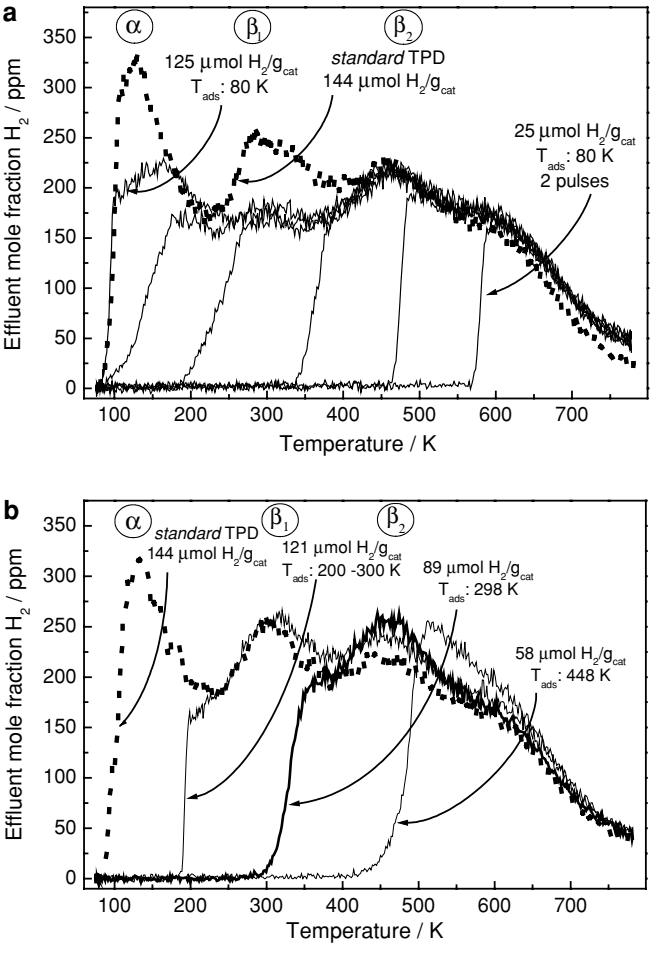

FIG. 7. TPD experiments subsequent to dosing by means of pulse flow H_2 chemisorption up to saturation (a) and subsequent to H_2 dosing at different T_{ads} (b). Experimental conditions: β = 10 K min^{-1}; Q_{He} = 50 ml (STP) min^{-1}.

profile is achieved, which was found in experiments subsequent to dosing H_2 at 78 K (cf. traces A and B in Fig. 6). A slightly changed pretreatment compared to the standard method led to the TPD profiles displayed in Fig. 7b: H_2 was dosed at three different temperatures (448, 300, and 300 K, followed by cooling to 200 K). Then, the catalyst was cooled to 78 K in He instead of H_2. Hence, the fraction of weakly bound hydrogen is flushed out during this pretreatment. The sudden generation of gas-phase H_2 in the effluent (Fig. 7b) is caused by recombination of those hydrogen species which remained on the surface at the chosen dosing temperature. The peaks increased slightly in these experiments compared to the ones obtained in the standard H_2 TPD experiment. This phenomenon can be explained by a low activation barrier which exists for a few additional adsorption sites (cf. previous paragraph).

3.2. Volumetric Hydrogen Chemisorption

Volumetric H_2 chemisorption at room temperature is applied as a standard technique to determine metal surface areas (55). The application of transient operations has the advantage that significantly more information about metallic sites becomes available. In our study, a significant amount of adsorbed hydrogen recombinatively desorbed in the TPD experiment below 300 K, which is the standard operating temperature for static chemisorption. Hence, strong emphasis is placed on the correlation between the α, β_1, and β_2 hydrogen detected in the TPD experiments and the amounts of weakly and strongly bound species determined by means of volumetric chemisorption.

Contrary to the transient TPD operation, volumetric chemisorption is carried out under isothermal conditions. Steady state between adsorption and desorption is established before a small amount of H_2 is additionally dosed stepwise under static conditions. Then, the hydrogen monolayer is determined by extrapolation of the linear part of the combined isotherm to zero pressure, $p_{H_2} = 0$ Pa (Fig. 8), yielding the amount 124 μmol g_{cat}^{-1}, which is divided into a weak contribution of 31 μmol g_{cat}^{-1} and a strong contribution of 93 μmol g_{cat}^{-1}, respresenting 25 and 75% of a hydrogen monolayer, respectively. The total amount is in very good agreement with the amount of H_2 adsorbed in the TPA experiment (119 μmol g_{cat}^{-1}; Fig. 4) and of H_2 desorbed in the TPD experiment subsequent to dosing H_2 at 78 K (118 μmol g_{cat}^{-1}; Fig. 6). Table 1 summarizes the experimental results obtained from volumetric chemisorption at 300 K on Ru/MgO catalysts with varying Ru loading. Here, n_{des} specifies the amount of H_2 desorbed in the TPD experiments (not shown here) above 300 K.

3.3. Thermal Treatment of the Catalyst

In order to investigate the influence of the thermal treatment on the shape of the TP spectra, a series of TPD experiments was carried out subsequent to the treatment at

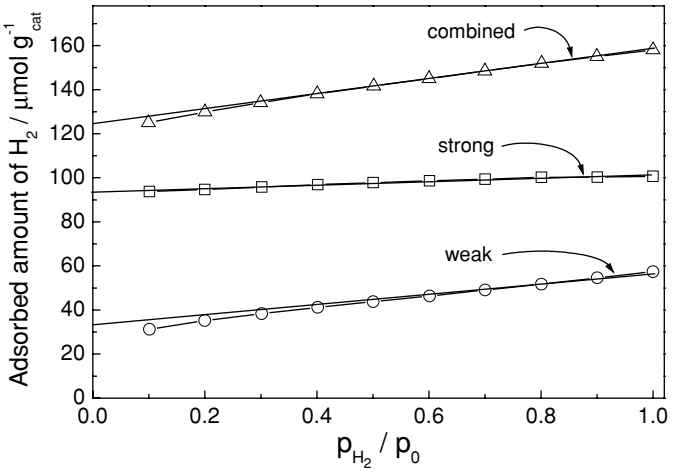

FIG. 8. Results of the volumetric hydrogen chemisorption at room temperature for 3.3 wt% Ru/MgO (imp).

different temperatures. The Ru/MgO catalyst was heated stepwise in ammonia synthesis feed gas starting at 783 K and going up to 1330 K. Subsequently, the catalytic activity was measured, and a standard H_2 TPD experiment followed. The difference in the two XRD patterns is shown in Fig. 9. The diffraction pattern of the sample, which was treated up to a temperature of 783 K (lower XRD pattern), reveals only the presence of highly crystalline MgO. By means of H_2 chemisorption a Ru mean particle size of 1.3 nm was calculated, which was confirmed by TEM. The lack of diffraction lines of Ru metal is, in view of these results, due to the presence of these small particles, because such a particle size lies below the detection limit of the diffractometer (>2 nm). In contrast, diffraction lines at $2\Theta = 38.5$ and 44° for the

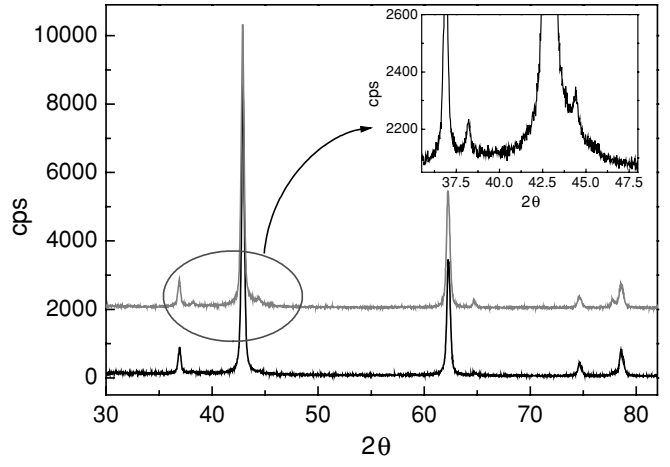

FIG. 9. XRD patterns of Ru/MgO before (lower pattern) and after sintering at 1330 K (upper pattern). The following reflections can be assigned to MgO (2Θ, relative intensity in brackets): 36.9 (4), 42.9 (100), 62.3 (39).

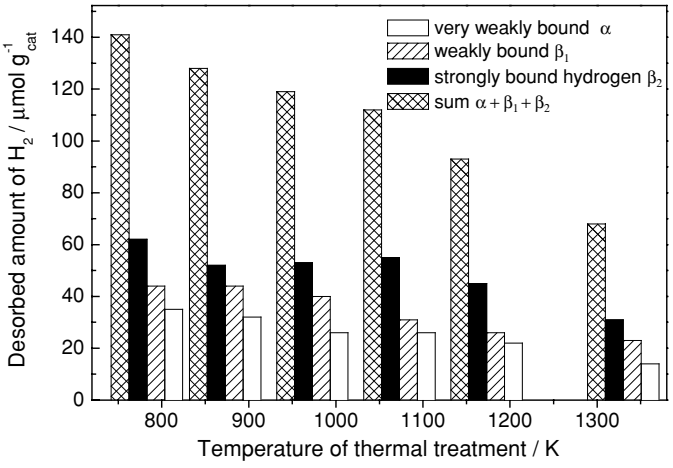

FIG. 10. Results after thermal treatment of the catalyst.

thermally treated sample (upper XRD pattern) become visible which can be assigned to Ru(100) and (101) lines (inset of Fig. 9).

The thermal treatment has no significant effect on the position of the TPD peaks. It can be seen from Fig. 10 that the total amount of active sites for H_2 adsorption diminished by about 50% when the thermal treatment temperature was further increased from 783 to 1330 K (144–68 µmol g_{cat}^{-1}). However, a slight decrease in the amount of α hydrogen and a corresponding increase in the β_2 peak can be detected, indicating a loss of defectlike sites.

3.4. Interaction of H_2 with a Cs-Promoted Ru/MgO Catalyst

For further investigations, TPD and TPA experiments under comparable reaction conditions were performed with a Cs-promoted Ru/MgO catalyst. Figure 11 (top) displays the results of the standard TPD using a heating rate of 2, 5, and 10 K min^{-1}. In contrast to the spectra obtained with the unpromoted catalyst (Fig. 2), a significant increase in β_1 hydrogen was observed, whereas a smaller amount of α hydrogen was detected. Furthermore, a strong impact of the promoter on the TPD spectrum was also found in the TPD experiment subsequent to dosing H_2 at 78 K (Fig. 11, bottom). As a reminder, these dosing conditions were applied for the unpromoted Ru/MgO catalyst, yielding a spectrum similar to that of the standard TPD experiment (Fig. 6). However, in the case of the Cs-promoted Ru/MgO catalyst H_2 adsorption was strongly suppressed (yielding only 70 instead of 170 µmol g_{cat}^{-1} in the standard TPD experiment), giving rise only to the high-temperature desorption peak.

Another striking phenomenon was observed in the TPA experiment (Fig. 11, middle): compared to the TPA spectrum for the unpromoted Ru/MgO catalyst an additional hydrogen uptake was detected in the TPA experiments, showing a maximum at around 130 K.

3.5. Microkinetic Modeling

Modeled second-order desorption signals based on the Langmuir isotherm using the Arrhenius law for the rate constants are symmetric and shift to higher temperatures with increasing heating rates. It can be seen from our experimental results that the peaks were generally broadened. They showed a tailing toward higher temperatures and their

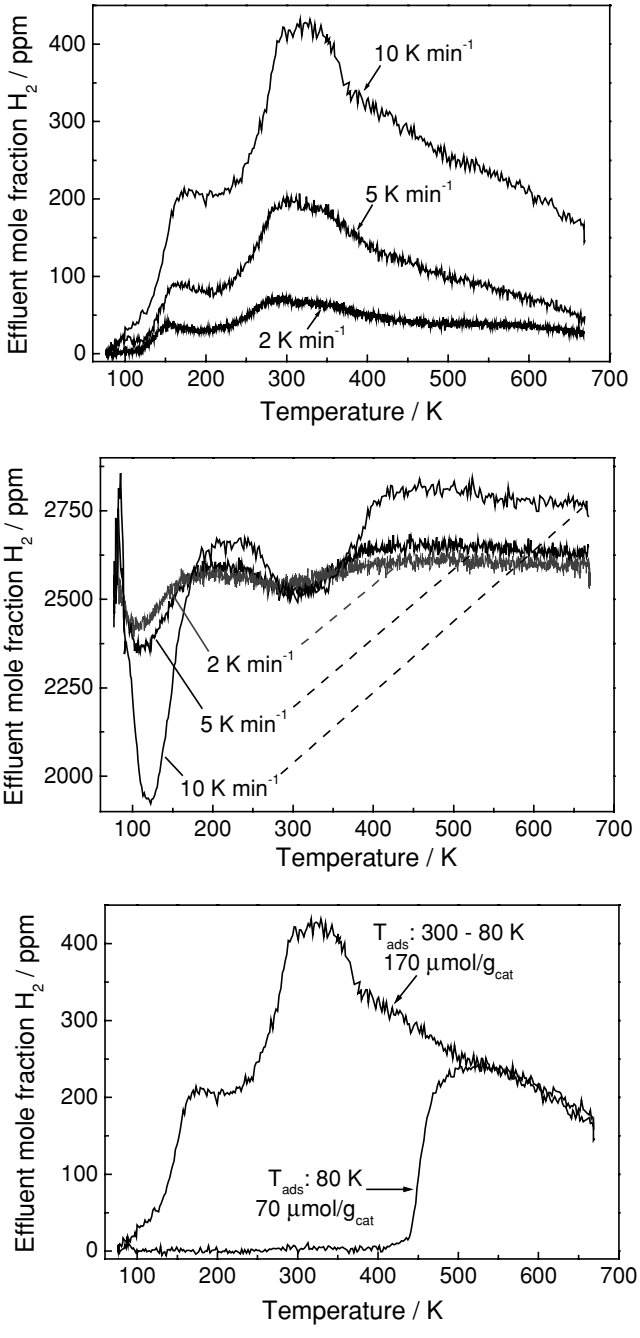

FIG. 11. Standard TPD spectra (top), TPD experiment subsequent to H_2 dosing at 78 K (bottom), and TPA spectrum (middle) for 3.3 wt% Cs–Ru/MgO.

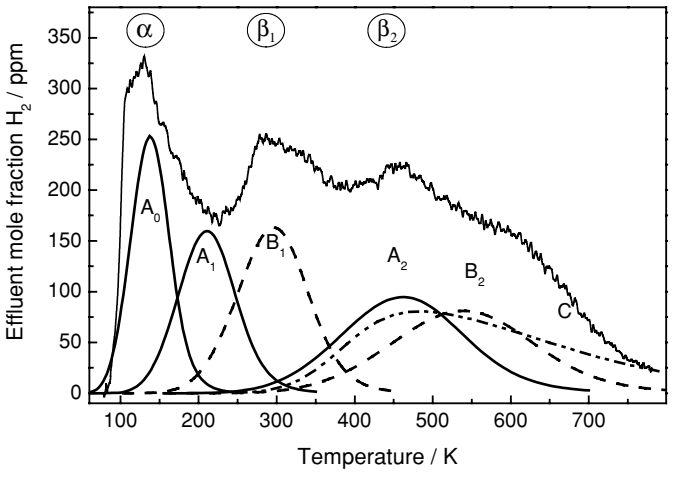

FIG. 12. Microkinetic analysis of the desorption signals of the standard H_2 TPD spectrum. The notation in the figure and the parameters are taken from Table 3. Model for contribution C was taken from Ref. (31).

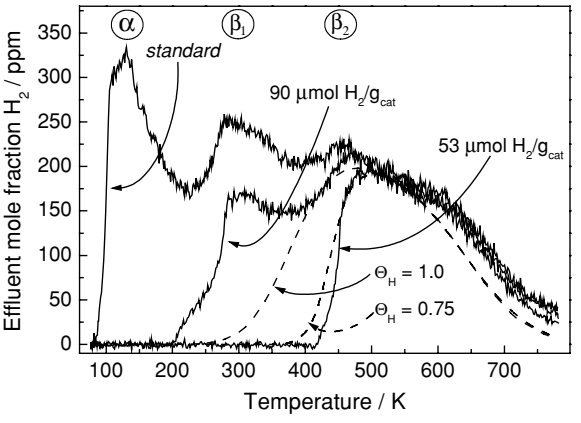

FIG. 13. TPD experiments subsequent to dosing H_2 by means of a 2300-ppm H_2/He mixture compared to the standard H_2 TPD experiment. Different initial coverages of adsorbed hydrogen (Θ_H) were achieved by varying the dosing time at 78 K. Experimental conditions: $\beta = 10$ K min^{-1}; $Q_{He} = 50$ ml (STP) min^{-1}. Dashed traces represent the modeled second-order desorption signals based on the model given in Ref. (31).

maxima shifted only slightly toward higher temperatures with increasing heating rates. In contrast to the expected ideal behavior, these differences can be attributed to two effects: on the one hand, repulsive interactions among the hydrogen atoms in the adsorbate layer take place, and on the other, readsorption occurs in the catalytic bed, which strongly influences the desorption process and, thus, alters the form and position of the desorption signals significantly.

In order to bridge the material and the pressure gaps, we aimed at assigning the three peaks in the TPD spectra to the desorption from Ru single-crystal surfaces. In a first simple approach, shown in Fig. 12, the three well-defined surfaces Ru(0001), Ru(10$\bar{1}$0), and Ru(11$\bar{2}$1) were assumed to make a contribution to the desorption spectra obtained from the Ru/MgO catalyst (Table 3). In the model, the microreactor was simulated as a continuously stirred tank reactor (CSTR). The reaction rate of the elementary step for each site is expressed as

$$\frac{d\Theta_H}{dt} = 2A_{ads} \cdot e^{-\frac{E_{ads}}{RT}} \cdot p_{H_2} \cdot (1-\Theta_H)^2 - 2A_{des} \cdot e^{-\frac{E_{des}}{RT}} \cdot \Theta_H^2, \quad [1]$$

whereas Θ_H represents the fractional coverage of each site up to $\Theta_H = 1$ at complete saturation.

In general, the kinetic parameters of the elementary steps summarized in Table 3 were taken from the literature when available or estimated based on transition state theory (59); e.g., for the second-order desorption of hydrogen, a preexponential factor A_{des} of 1.0×10^{13} s^{-1} was assumed. Since the adsorption was found to proceed without an activation barrier, E_{ads} was set to be 0 kJ mol^{-1} for all contributions. Hence, readsorption is only governed by the value for A_{ads}. Finally, the activation energy of desorption was fixed for the contributions A and B, but a coverage-dependency for C was introduced to adopt repulsive interactions among the hydrogen species. Simulation details for the underlying model are given in Refs. (31, 60). The main contribution to the low-temperature TPD signal can be attributed to species desorbing from more open surfaces, whereas the broad high-temperature part arises from the desorption from basal planes. The striking result is the good agreement between the experimental data and the simulated curves in the case of β_2 hydrogen for two different initial coverages of Θ_H (Fig. 13).

TABLE 3

Microkinetic Analysis of the Desorption Signals of the Standard H_2 TPD Spectrum

Single-crystal peaks	Ru(11$\bar{2}$1) A_0	Ru(11$\bar{2}$1) A_1	Ru(10$\bar{1}$0) B_1	Ru(11$\bar{2}$1) A_2	Ru(10$\bar{1}$0) B_2	Ru(0001) C
E_{des} (kJ mol^{-1})	20	31	50	70	82	92–123
A_{des} (s^{-1})	10^{13}	10^{13}	8×10^{13}	10^{13}	5×10^{12}	3×10^{15}
Fraction of the signal (%)	12.5	12.5	15.5	15.5	22	22
$n_{Ru} \times 10^{18}$	4	4	6	6	7.4	7.4
s_0	0.5	0.5	0.5	0.5	0.5	0.5
k_{ads} ((Pa s)$^{-1}$)	11,000	11,000	6,000	11,000	6,000	3,441

4. DISCUSSION

4.1. Energetics of the Interaction of H_2

For the interpretation of the TPD spectra in terms of elementary-step kinetics it is fundamental to know how the adsorption process takes place. In our study, there was no indication of the presence of physisorbed H_2-$*$ in the applied temperature range. This observation is also in good agreement with results obtained by inelastic neutron scattering measurements on a carbon-supported ruthenium catalyst by Mitchell *et al.* (61). They identified physisorbed hydrogen at a temperature of 23 K. In general, hydrogen adsorption on transition metal is thought to be nonactivated (62). From adsorption studies on Ru single crystals (23, 27) it can be deduced that H_2 dissociatively adsorbs nearly without an activation barrier ($E_{ads} = 0$ kJ mol^{-1}). Our H_2 TPA experiments described in Section 3.1.2 confirmed that the dissociation proceeds without an activation barrier. Hence, we refer to the hydrogen species detected in the spectra as dissociatively chemisorbed H-$*$ species.

Nevertheless, repulsive interaction among the hydrogen atoms is not the only reason for the broadening of the peaks. The second phenomenon, which appears to have a strong influence on the form of the signal and on the peak positions, is readsorption. Gas-phase H_2 desorbed from the catalyst is carried by helium through the catalytic bed, and since the adsorption of H_2 on Ru/MgO is a nonactivated process, it can easily adsorb on free surface sites. Thus, desorption and readsorption take place until the hydrogen molecules finally reach the end of the catalyst bed. The interactions are more pronounced at higher temperatures, where more free surface sites are available for readsorption, causing a broadening of the desorption peaks and a shift toward higher temperatures. Engelke *et al.* (63) detected readsorption and hydrogen interparticle motion by means of line broadening in NMR measurements when investigating H_2 adsorption on Ru/SiO_2.

The TPD spectra presented in this study are comparable to the H_2 TD spectra obtained with single-crystal surfaces (23, 30). On Ru(0001), the spectra showed a low-temperature peak with a broad shoulder tailing toward higher temperatures. Jachimowski *et al.* [31] interpreted this characteristic shape in terms of repulsive interactions between adsorbate atoms and their neighbor and next-neighbor atoms (31). A maximum of 1.42 hydrogen adatoms per unit cell ($\Theta = 1.42$) was achieved by using gas-phase atomic hydrogen (33). The amount of 144 μmol H_2 g_{cat}^{-1} desorbed in our standard TPD experiment corresponds to an average hydrogen coverage of $\Theta_H = 1.2$. This value is calculated on the base of 124 μmol g_{cat}^{-1} determined by means of volumetric H_2 chemisorption, which is per definition equivalent to a hydrogen monolayer ($\Theta_H = 1.0$; cf. Section 3.3). It can be seen from the results of Jachimowski *et al.* (31) that at a coverage of $\Theta_H = 1.2$ neighbor–neighbor and other repulsive interactions became significant (31). On Ru(0001) and Ru(10$\bar{1}$0), these interactions cause a Z-shaped dependence of the activation energy of desorption, E_{des}, on the coverage Θ_H (17, 64). A similar trend was observed for Ru/MgO. At high hydrogen coverages, intensive repulsions occurred among the hydrogen atoms and, in turn, E_{des} was lower and, correspondingly, hydrogen desorbed at lower temperatures in the TPD experiment. With decreasing coverage the repulsive interactions decrease, and the hydrogen layer reorganizes, forming more-stable adsorbate structures (e.g., on the Ru(0001) surface: $\Theta = 0.35, \sqrt{3}$; $\Theta = 0.5, p(2\times1)$H; $\Theta = 0.75, 2\times2-3$H (30)). Thus, E_{des} increased and the desorption temperature was found to shift to higher values. The hydrogen coverage is now lower than at the beginning of the desorption process and, correspondingly, the amount of adsorbed H_2 diminished, resulting in a formation of a shoulder in the signal.

4.2. Comparison between Static and Transient Experiments

In a TPD experiment subsequent to dosing, the catalyst is flushed in a flow of He to remove H_2 from the gas phase before starting the heating procedure. A fraction of the very weakly bound hydrogen may have already desorbed and is removed by the carrier gas, since p_{H_2} is lower than under dosing conditions. By means of the TP methods the amount of adsorbed H_2 is determined indirectly, only taking the amount of desorbed species into account. A possible loss of hydrogen species during flushing is therefore not considered. In contrast, the volumetric chemisorption allows direct detection of the amount of H_2 adsorbed under dosing conditions. Thus, also the amount of very weakly bound species can be determined. This is well demonstrated by the results of the volumetric chemisorption performed at 78 K, where 97 μmol g_{cat}^{-1} of weakly bound hydrogen was determined (cf. Table 2), which was missing in any TP experiments. Even in the TPA experiment at a higher hydrogen partial pressure this amount was not detected, since saturation coverage was reached by adsorbing 119 μmol g_{cat}^{-1}. Due to the good agreement of the values for n_{des} and the strongly bound hydrogen it is safe to propose that the strongly bound hydrogen identified by the volumetric chemisorption can be quantitatively correlated to those hydrogen species detected in the TPD spectra above the dosing temperature at which the volumetric chemisorption was carried out.

Hydrogen spillover is sometimes observed on supported catalysts, which, in turn, would lead to an overestimation of our results. Even when dosing H_2 at a constant temperature between 783 and 300 K, no indications for any significant hydrogen respillover were found, as was described for the system Ru/Al_2O_3 (65). Under the treatment conditions employed in the present work, the influence of the MgO

support on the H_2 adsorption can also be neglected. To the best of our knowledge, H_2 adsorption on MgO was detected only after thermal treatment at 1123 K (66). The formation of subsurface hydrogen is also very unlikely, since the Ru particles are too small (1.3-nm diameter) to have significant contributions from the bulk. This is in agreement with Shi and Jacobi, who did not find any indication for the existence of subsurface hydrogen for Ru(0001) (30).

4.3. Thermal Treatment of the Catalyst

In general, three phenomena may occur during thermal treatment of metal catalysts (67): phase transformations, growth of the metal particles, and strong metal–support interactions (SMSI). The increase in particle size corresponds to a loss of active surface area, since the agglomeration of smaller metal crystallites to the more stable large particles leads to a lower surface-to-volume ratio. This growth occurs either by a migration of single atoms (atomic migration) or by a coalescence of two or more small crystallites to a bigger one (crystallite migration).

The decrease in the measured BET surface area by 40%, from 50 to 31 $m^2\ g_{cat}^{-1}$, is accompanied by a loss in micropore volume. Both observations point to a change in the structure of the MgO support. Nevertheless, SMSI cannot be excluded reliably. Since the Ru particle size is very small, a possible formation of Mg ruthenates would not be determined by means of XRD. During the sintering procedure, a growth of the metal particle size corresponding to a continuous decrease in the peaks in the TPD spectra was observed. Based on XRD measurements (Fig. 9) an increase in average ruthenium particle size from below 2 to around 26 nm was estimated. The low intensity of the relatively broad reflections and the overlap with the reflex of the MgO originating at 44° 2Θ lowers the precision of the line broadening analysis. Hence, the value of 26 nm should be regarded as an overestimate of the real number. By means of volumetric hydrogen chemisorption and assuming a Ru : H stoichiometry of 1 : 1 (55–57), the specific metal surface area after sintering was determined to be $4\ m^2\ g_{cat}^{-1}$. Taking a total loading of Ru on the catalyst (3.3 wt%) into account leads to an average particle size of 4 nm. Accordingly, the dispersion decreased from 70 to 24%.

For the study of the interaction of H_2 with the catalyst the applied maximum temperature of 783 K turned out to be the optimum. An activation up to temperatures below 783 K yielded lower values for the amount of adsorbed H_2 (573 K, 132 $\mu mol\ g_{cat}^{-1}$; 673 K, 135 $\mu mol\ g_{cat}^{-1}$), presumably due to the presence of oxide species on the surface. Activation at temperatures above 783 K led to a loss of active sites for H_2 chemisorption, as described above. However, the turnover frequency for ammonia synthesis increases, while the specific surface area decreases slightly (Table 4). Recently, Hinrichsen *et al.* (68) have shown that only a small fraction of the exposed Ru atoms on Ru/MgO is highly active for the dissociative adsorption of dinitrogen. Since this elementary step is rate limiting in ammonia synthesis, it can reasonably be assumed that only a few Ru sites are active for the overall reaction (68, 69). Recent work by Dahl and co-workers (70) suggests that special sites of a B_5 geometry are primarily responsible for the high catalytic activity on Ru clusters. Hence, the above-mentioned increase in observed ammonia synthesis activity could be explained by an increase in the total number of B_5-type sites formed during thermal treatment at higher activation temperatures.

TABLE 4

Turnover Frequencies for Ammonia Synthesis after Thermal Treatment of the Ru/MgO Catalyst at Various Temperatures

T (K)	T_{sinter} (K)	x_{NH_3} (ppm)	$n_{Ru,s}$ ($\mu mol \cdot g_{cat}$)	r^{TOF} (s^{-1})
573	573	120	132	3.38×10^{-5}
663	673	1540	135	4.24×10^{-4}
583	783	576	141	1.52×10^{-4}
663	783	2488	141	6.56×10^{-4}
663	873	2585	128	7.51×10^{-4}
663	973	2671	119	8.34×10^{-4}

4.4. Bridging the Pressure and Material Gaps

The low-temperature peak in the standard TPD experiments can be assigned to the desorption of α hydrogen (modeled curve A_0 in Fig. 12) from twofold coordinated adsorption sites on rough single crystal surfaces and from low coordination sites such as edges, defects, or kinks. They play an important role in H_2 adsorption according to the description by King and co-workers of a "portal"-mediated adsorption (43, 71). According to our microkinetic analysis, the peak assigned to the α hydrogen represents hydrogen species desorbing with an E_{des} of 20 kJ mol^{-1} or even lower, since only H_2 desorbing above 78 K was detected. Narayan and King (43) determined by means of microcalorimetry an E_{des} of about 10 kJ mol^{-1}. However, a direct comparison is difficult since the dispersion and activation procedure, which is important for the formation of defects, differs for both catalyst systems.

The largest fraction (44%) desorbs as β_2 hydrogen (modeled curves A_2, B_2, and C in Fig. 12) in the TPD experiments. Values for E_{des} of 70 kJ, 80 kJ, and 92–123 kJ mol^{-1} were determined to be in good agreement with results for the fcc sites on Ru(10$\bar{1}$0), Ru(11$\bar{2}$1), and Ru(0001), respectively. On Ru(0001), E_{des} was found to vary strongly, with surface coverage in the range of 92–123 kJ mol^{-1} (30, 31). Since the fcc sites are thermodynamically most stable and represent the largest fraction of sites on Ru(0001), the contribution to the high-temperature peak can be assigned to the desorption from fcc sites of this surface. The other major contribution to this peak is due to the existence of fcc sites on

Ru(10$\bar{1}$0) and Ru(11$\bar{2}$1). The contribution for the β_1 peak (A_1 and B_1 in Fig. 12) can be assigned to the population of hcp sites of Ru(11$\bar{2}$1) and Ru(10$\bar{1}$0). Here, the values for E_{des} have been determined on Ru(11$\bar{2}$1) to be 31 kJ mol^{-1} and on Ru(10$\bar{1}$0) to be 56 kJ mol^{-1} (27, 36, 37, 64). Analysis of the microcalorimetric data obtained by the King group for H_2 adsorption on Ru/SiO_2 led to a heat of adsorption varying from 90 to 50 kJ mol^{-1} for the strongly and weakly bound species, respectively (40).

Based on the experimental observations combined with the modeling results, the process of the H_2 adsorption on Ru/MgO can be described according to the portal-mediated adsorption proposed by the King group (43, 71): gas-phase H_2 preferentially dissociates on the low-coordinated defectlike sites producing the very weakly bound hydrogen species. These highly mobile hydrogen species diffuse to high-energy sites, leading to β_2 hydrogen, and then fill up intermediate-energy sites, leading to β_1 hydrogen. A fraction of weakly bound hydrogen species desorbs directly when flushing the setup with He after the adsorption procedure. This conjecture is supported by means of microkinetic modeling using the equations reported in Ref. (31) and transferring them to the conditions applied in our experiment (Fig. 13). When the fractional coverage of the β_2 sites increased from 0.75 to 1.0, the onset of the signal was found to shift toward lower temperatures, as is known to occur for second-order desorption. The presented results, particularly when the results from the TPD experiments subsequent to H_2 dosing at 78 K are considered, also clearly show that a second pathway should be included to allow the direct adsorption on the basal planes, which especially occurs at higher temperatures. A similar two-pathway mechanism was proposed for H_2 adsorption on single crystals by Bernasek and Somorjai (72). They reported that stepped Pt(997) and Pt(553) surfaces were approximately 100 times more active for the isotopic H_2/D_2 exchange reaction than were Pt(111) surfaces.

The results obtained with the Cs-promoted catalyst corroborate the model of portal-mediated adsorption. Key to understanding the microscopic processes is the role the localization of the promoters plays. Based on calculations, Hoost and Goodwin (73) found that potassium selectively decorates surface sites on a Ru/SiO_2 catalyst. *In situ* surface characterization tools, such as atomic-resolution transmission electron microscopy in the presence of reactive gases and at high temperatures, are becoming available to clarify how a promoter enhances the activity of the catalyst (74, 75). From our kinetic results it can be concluded that the fast path via edges, corners, and low-coordinated sites is blocked by the dopant. The results clearly reveal that more sites are filled by dosing H_2 at 300 K followed by cooling to 78 K, whereas the dissociative adsorption is slowed when H_2 is dosed at 78 K. Correspondingly, an additional uptake of H_2 was found in the TPA experiment at 150 K. This observation suggests the existence of an activation barrier which is surmounted using the higher dosing temperature applied in the standard TPD. Further studies are in progress to gain deeper insight into the microkinetics of activated adsorption for the Cs-promoted catalyst system and to study the role of coadsorbates such as O-$*$ and N-$*$ for unpromoted Ru catalysts.

5. CONCLUSIONS

The application of volumetric hydrogen chemisorption and temperature-programmed techniques was shown to yield similar results. As a result of the microkinetic analysis, a correlation between the amount of desorbing hydrogen detected in the TP experiments and the amount of hydrogen species measured by means of volumetric hydrogen chemisorption at different constant temperatures was obtained.

When dosing H_2 by cooling it in a flow of pure H_2 from 300 to 78 K followed by heating the Ru/MgO catalyst in He with a linear heating rate (the so-called standard H_2 TPD experiment), the spectrum displayed three well-resolved H_2 desorption peaks: a sharp, steep peak with a maximum at 120 K, which can be assigned to the desorption of so-called very weakly bound α hydrogen; one with a maximum at 300 K (weakly bound β_1 hydrogen); and a broad one at around 450–600 K (strongly bound β_2 hydrogen). The interaction of H_2 with a reduced adsorbate-free Ru/MgO catalyst is therefore an example of a nonactivated dissociative "portal"-mediated adsorption process: hydrogen prefers to dissociatively adsorb on low-coordinated defectlike sites, producing very weakly bound, highly mobile hydrogen species. These species migrate to sites that adsorb hydrogen most strongly ($\Delta H_{ads} > 70$ kJ mol^{-1}), followed by populating intermediate-energy sites (20 kJ mol$^{-1} < \Delta H_{ads} < 70$ kJ mol^{-1}) and low-energy sites ($\Delta H_{ads} < 20$ kJ mol^{-1}). In addition, Cs was found to selectively decorate defectlike sites suppressing the fast adsorption path based on the model of the portal-mediated adsorption.

Various TP experiments (TPD, TPA) were carried out applying different hydrogen dosing procedures (e.g., flow pulse chemisorption, dosing temperature). The subsequent spectra differed in the position and the form of the peaks due to phenomena such as repulsive interactions in the adsorbate layer and readsorption along the catalytic bed. By means of microkinetic modeling it was found that the low-temperature peak can be assigned to the desorption of α hydrogen from twofold coordinated adsorption sites on open single-crystal surfaces and from low-coordination sites such as edges, defects, or kinks. Obviously, there is an overlap of different desorption processes for the high-temperature peak (β_2 hydrogen). Contributions could be assigned to hydrogen species desorbing from the fcc sites on Ru(0001) Ru(10$\bar{1}$0), and Ru(11$\bar{2}$1) single-crystal surfaces. The peak

attributed to β_1 hydrogen is due to the population of the hcp sites on these single-crystal surfaces.

Finally, the stepwise thermal treatment of the catalyst up to 1330 K caused a growth in metal particle size corresponding to a continuous decrease in peaks in the TPD spectra. There were also indications of a modification of the support: the BET surface area decreased about 40% and a loss in the number of micropores was additionally observed. The thermal treatment experiments confirmed 783 K as the optimum temperature for the catalyst activation before H_2 TPD experiments.

ACKNOWLEDGMENTS

The authors gratefully acknowledge the Deutsche Forschungsgemeinschaft (DFG) for the financial support within the Graduiertenkolleg "Dynamic Processes at Solid Surfaces—Adsorption, Desorption, Heterogeneous Catalysis" in Bochum. We benefited from fruitful discussions with H. Bielawa, who prepared the catalysts. We would like to thank S. Wiedemeyer and V. Hagen for measuring the volumetric hydrogen chemisorption, M. Schoen for recording the XRD spectra, and K. Keppler for carrying out the ICP analyses.

REFERENCES

1. Vannice, M. A., *Catal. Rev.–Sci. Eng.* **14**, 153 (1976).
2. Schulz, H., *Appl. Catal. A* **186**, 3 (1999).
3. van der Laan, G. P., and Beenackers, A. A. C. M., *Catal. Rev.–Sci. Eng.* **41**, 255 (1999).
4. Shires, P. J., Cassata, J. R., Mandelik, B. G., and Dijk, C. P. van, U.S. Patent 4,479,925 (assigned to M. W. Kellogg) (1984).
5. Benner, G. S., Blanc, J. R. Le, Lee, J. M., Leftin, H. P., Shires, P. J., and Dijk, C. P. van, U.S. Patent 4,568,532 (assigned to M. W. Kellogg) (1986).
6. Czuppon, T. A., Knez, S. A., Schneider, R. W., and Worobets, G., *Ammonia Plant Saf. Relat. Facil.* **34**, 236 (1994).
7. Rhodes, A. K., *Oil Gas J.* **11**, 37 (1996).
8. Strait, R., *Nitrog. Methan.* **238**, 37 (1999).
9. Bielawa, H., Hinrichsen, O., Birkner, A., and Muhler, M., *Angew. Chem.* **113**, 1093 (2001); *Angew. Chem. Int. Ed.* **40**, 1061 (2001).
10. Jacobsen, C. J. H., *J. Catal.* **200**, 1 (2001).
11. Vannice, M. A., *J. Catal.* **37**, 449 (1975).
12. Bajusz, I.-G., and Goodwin, J. G., Jr., *J. Catal.* **169**, 157 (1997).
13. Hornung, A., Muhler, M., and Ertl, G., *Top. Catal.* **11/12**, 263 (2000).
14. van der Steen, P. J., and Scholten, J. J. F., *Appl. Catal.* **58**, 281 (1990).
15. van der Steen, P. J., and Scholten, J. J. F., *Appl. Catal.* **58**, 291 (1990).
16. Patzlaff, J., and Gaube, J., *Chem.-Ing.-Tech.* **69**, 1462 (1997).
17. Shimizu, H., Christmann, K., and Ertl, G., *J. Catal.* **61**, 412 (1980).
18. Danielson, L. R., Dresser, M. J., Donaldson, E. E., and Dickinson, J. T., *Surf. Sci.* **71**, 599 (1978).
19. Barteau, M. A., Broughton, J. Q., and Menzel, D., *Surf. Sci.* **133**, 443 (1983).
20. Conrad, H., Scala, R., Stenzel, W., and Unwin, R., *Surf. Sci.* **145**, 1 (1984).
21. Yates, J. T., Jr., Peden, C. H. F., Houston, J. E., and Goodman, D. W., *Surf. Sci.* **160**, 37 (1985).
22. Hofmann, P., and Menzel, D., *Surf. Sci.* **152/153**, 382 (1985).
23. Feulner, P., and Menzel, D., *Surf. Sci.* **154**, 465 (1985).
24. Feulner, P., Pfnür, H., Hofmann, P., and Menzel, D., *Surf. Sci.* **173**, L576 (1986).
25. Lindroos, M., Pfnür, H., and Menzel, D., *Surf. Sci.* **192**, 421 (1987).
26. Lindroos, M., Pfnür, H., Feulner, P., and Menzel, D., *Surf. Sci.* **180**, 237 (1987).
27. Lauth, G., Schwarz, E., and Christmann, K., *J. Chem. Phys.* **91**, 3729 (1989).
28. Sokolowski, M., Koch, T., and Pfnür, H., *Surf. Sci.* **243**, 261 (1991).
29. Held, G., Pfnür, H., and Menzel, D., *Surf. Sci.* **271**, 21 (1992).
30. Shi, H., and Jacobi, K., *Surf. Sci.* **313**, 289 (1994).
31. Jachimowski, T. A., Meng, B., Johnson, D. F., and Weinberg, W. H., *J. Vac. Sci. Technol. A* **13**, 1564 (1995).
32. Fan, C. Y., and Jacobi, K., *Surf. Sci.* **482–485**, 21 (2001).
33. Jachimowski, T. A., and Weinberg, W. H., *J. Chem. Phys.* **101**, 10997 (1994).
34. Christmann, K., and Muschiol, U., *Z. Phys. Chem.* **197**, 155 (1996).
35. Gruyters, M., and Jacobi, K., *J. Electron Spectrosc. Relat. Phenom.* **64/65**, 591 (1993).
36. Döll, R., Hammer, L., Heinz, K., Bedürftig, K., Muschiol, U., Christmann, K., Seitsonen, A. P., Bludau, H., and Over, H., *J. Chem. Phys.* **108**, 8671 (1998).
37. Dietrich, H., Jacobi, K., and Ertl, G., *J. Chem. Phys.* **105**, 8944 (1996).
38. Engelke, F., Bhatia, S., King, T. S., and Pruski, M., *Phys. Rev. B* **49**, 2730 (1994).
39. Uner, D. O., Pruski, M., and King, T. S., *J. Catal.* **156**, 60 (1995).
40. Narayan, R. L., Savargaonkar, N., Pruski, M., and King, T. S., *Stud. Surf. Sci. Catal.* **101**, 921 (1996).
41. Uner, D. O., Savargoankar, N., Pruski, M., and King, T. S., *Stud. Surf. Sci. Catal.* **109**, 315 (1997).
42. Savargoankar, N., Narayan, R. L., Pruski, M., Uner, D. O., and King, T. S., *J. Catal.* **178**, 26 (1998).
43. Narayan, R. L., and King, T. S., *Thermochim. Acta* **312**, 105 (1998).
44. Kumar, N., King, T. S., and Vigil, D., *Chem. Eng. Sci.* **55**, 4973 (2000).
45. Izumi, Y., Hoshikawa, M., and Aika, K.-I., *Bull. Chem. Soc. Jpn.* **67**, 3191 (1994).
46. Kubota, J., and Aika, K.-I., *J. Chem. Soc. Chem. Commun.* 661 (1992).
47. Muhler, M., Rosowski, F., and Ertl, G., *Catal. Lett.* **24**, 317 (1994).
48. Aika, K., Takano, T., and Murata, S., *J. Catal.* **136**, 126 (1992).
49. Lu, K., and Tatarchuk, B. J., *J. Catal.* **106**, 166 (1987).
50. Shiflett, W. K., and Dumesic, J. A., *Ind. Eng. Chem. Fundam.* **20**, 246 (1981).
51. Murata, S., and Aika, K.-I., *Appl. Catal. A* **82**, 1 (1992).
52. Rosowski, F., Hornung, A., Hinrichsen, O., Herein, D., Muhler, M., and Ertl, G., *Appl. Catal. A* **151**, 443 (1997).
53. Bielawa, H., Kurtz, M., Genger, T., and Hinrichsen, O., *Ind. Eng. Chem. Res.* **40**, 2793 (2001).
54. Bielawa, H., Ph.D. thesis. Ruhr-Universität, Bochum, 2000.
55. Dalla Betta, R. A., *J. Catal.* **34**, 57 (1974).
56. Goodwin, J. G., Jr., *J. Catal.* **68**, 227 (1981).
57. Sun, Y.-K., and Weinberg, W. H., *Surf. Sci.* **214**, L246 (1989).
58. Anderson, J. R., and Pratt, K. C., "Introduction to Characterization and Testing of Catalysts." Academic Press, New York, 1985.
59. Dumesic, J. A., Rudd, D. F., Aparicio, L. M., Rekoske, J. E., and Treviño, A. A., "The Microkinetics of Heterogeneous Catalysis," ACS Professional Reference Book. Am. Chem. Soc., Washington, DC, 1993.
60. Hinrichsen, O., Rosowski, F., Muhler, M., and Ertl, G., *Stud. Surf. Sci. Catal.* **109**, 389 (1997).
61. Mitchell, P. C. H., Parker, S. F., Tomkinson, J., and Thompsett, D., *J. Chem. Soc. Faraday Trans.* **94**, 1489 (1998).
62. Christmann, K., *Surf. Sci. Rep.* **9**, 1 (1988).
63. Engelke, F., Vincent, R., King, T. S., and Pruski, M., *J. Chem. Phys.* **101**, 7262 (1994).
64. Lauth, G., Ph.D. thesis. FU, Berlin, 1989.
65. Rosowski, F., Ph.D. thesis. FU, Berlin, 1996.
66. Ito, T., Sekino, T., Moriai, N., and Tokuda, T., *J. Chem. Soc. Faraday Trans. I* **77**, 2181 (1981).

67. Forzatti, P., and Lietti, L., *Catal. Today* **52**, 165 (1999).
68. Hinrichsen, O., Rosowski, F., Hornung, A., Muhler, M., and Ertl, G., *J. Catal.* **165**, 33 (1997).
69. Rosowski, F., Hinrichsen, O., Muhler, M., and Ertl, G., *Catal. Lett.* **36**, 229 (1996).
70. Jacobsen, C. J. H., Dahl, S., Hansen, P. L., Törnqvist, E., Jensen, L., Topsøe, H., Prip, D. V., Møenshaug, P. B., and Chorkendorff, I., *J. Mol. Catal. A* **163**, 19 (2000).
71. VanderWiel, D. P., Pruski, M., and King, T. S., *J. Catal.* **188**, 186 (1999).
72. Bernasek, S. L., and Somorjai, G. A., *J. Chem. Phys.* **62**, 3149 (1975).
73. Hoost, T. E., and Goodwin, J. G., Jr., *J. Catal.* **130**, 283 (1991).
74. Campbell, C. T., *Science* **294**, 1471 (2001).
75. Hansen, T. W., Wagner, J. B., Hansen, P. L., Dahl, S., Topsøe, H., and Jacobsen, C. J. H., *Science* **294**, 1508 (2001).